Heliyon 5 (2019) e02303

Contents lists available at ScienceDirect

Heliyon

journal homepage: www.heliyon.com

Thermally stratified flow of Jeffrey fluid with homogeneous-heterogeneous reactions and non-Fourier heat flux model

M. Ijaz *, M. Ayub

Department of Mathematics, Quaid-I-Azam University 45320, Islamabad, 44000, Pakistan

ARTICLE INFO

Keywords:
Mechanical engineering
Mechanics
Nonlinear physics
Thermodynamics
Homogeneous/heterogeneous reactions
Stagnation-point flow
Cattaneo-Christov heat flux

ABSTRACT

This article investigates the mixed convective flow of Jeffrey fluid near the axisymmetric stagnation point over an inclined permeable stretching cylinder. Analysis subjected to Cattaneo-Christov heat flux, thermal stratification and homogeneous-heterogeneous reactions are accounted. Suitable transformations are employed to obtain nonlinear ordinary differential system. Non-dimensional system is computed by Homotopy technique. Graphs and tables are constructed to analyze the influence of different flow parameters on temperature, concentration and velocity fields. The interpretation of skin friction coefficient is deliberated. It is noticed from obtained results that temperature is a decreasing function of thermal stratification parameter. Reverse behaviour of concentration is witnessed for higher estimations of homogeneous and heterogeneous parameters. Numerical results are compared with previous published results and found to be in good agreement for special casesof the emerging parameters.

1. Introduction

Study of nonlinear liquids has attained great importance due to its various applications in the fields of engineering and applied science. The complex characteristics of non-Newtonian fluids are not completely identified by single Navier-Stokes equation. In non-Newtonian fluids shear stress and shear rate are not linearly connected with each other therefore single constitutive equation is not enough to describe the relation between shear stresses and shear rate. Non-Newtonian liquids has a lot of applications in geophysics, petroleum procedures and chemical industry. Non-Newtonian liquids performs a vital role in chemical material (toothpastes, shampoos, cosmetics, grease, paints, pharmaceutical chemicals, oil reservoirs, etc.) food processing (fruit puree, mayonnaise, ketchup, milk, ice cream, alcoholic beverages, chocolates in liquefies form, yogurt, etc.) and in biological stuff (syrups, vaccines, synovial fluid, blood etc.) Such materials are categorized into integral, differential and rate types. The rate type materials can only be analysed through the impact of relaxation and retardation times. Relaxation and retardation times can be elucidated only through rate type materials. Jeffrey fluid [1, 2, 3, 4] is one of the subclasses of rate type materials describing the relaxation and retardation times effects. These features are present in complex polymeric flows and also in geological nuclear repositories [5]. Having this in mind, Hayat et al. [6] examined the radiative flow of Jeffrey liquid embedded in a porous medium with heat source/sink. Hussain et al. [7] studied the hydromagnetic flow of Jeffrey nanofluid within the frame thermal radiation and exponential stretching. Hayat et al. [8] discussed the Jeffrey fluid flow in view of Cattaneo-Christov heat flux and homogeneous/heterogeneous reaction. Tripathi et al. [9] analysed MHD peristaltic flow of Jeffrey liquid in a finite cylindrical tube. Reddy et al. [10] investigated the flow of Jeffrey liquid between two oscillating disks. Hamad et al. [11] explored the stagnation point flow of Jeffrey fluid subjected to variable thermal conductivity.

Heat transfer which is an important phenomenon in nature exists due to temperature difference within the same body or between two objects. Conventionally, heat transfer phenomena have been examined by Fourier's law [12]. But this law is not acceptable in a sense that any primary disturbance is felt instantly throughout the whole system. To overcome this difficulty Cattaneo [13] familiarised a thermal relaxation time in the traditional Fourier's law of heat conduction that allows the transport of heat via propagation of thermal waves with finite speed. Then Christov [14] has modified the Cattaneo law by introducing thermal relaxation time in terms of Oldroyd's upper-convective derivatives. This revised scheme is recognised as Cattaneo-Christov heat flux model. Ciarletta and Straughan [15] discussed the uniqueness of solution and structural stability of system through Cattaneo-Christov heat flux model. The thermal instability of flow through porous medium is analysed by Hadded [16] within the frame of Cattaneo-Christov model. This innovative study has

* Corresponding author.
E-mail address: misbahijaz@math.qau.edu.pk (M. Ijaz).

https://doi.org/10.1016/j.heliyon.2019.e02303
Received 27 February 2019; Received in revised form 18 June 2019; Accepted 9 August 2019
2405-8440/© 2019 Published by Elsevier Ltd. This is an open access article under the CC BY-NC-ND license (http://creativecommons.org/licenses/by-nc-nd/4.0/).

opened the modern era of research refs. [17, 18, 19, 20, 21, 22, 23].

Numerous reacting systems involve both homogeneous and heterogeneous reactions that respond differently in the presence or absence of a catalyst. Homogeneous and heterogeneous reactions occur in biochemical systems, combustion and catalysis. These reactions are also involved in nuclear reactor, biochemical system, industrial procedure, combustion etc. The physical change is completely identified from chemical reaction. Physical changes embrace changes of state, for example: ice liquefying to water and then converting to vapours. The physical properties of a substance will change during these phases, however its chemical identity will remain same. According to chemical reaction theory, chemical reactions are mainly classified as homogeneous and heterogeneous reactions. In homogeneous reactions, the reactants and products are in phase while in heterogeneous reactions both (reactants & products) are out of phase. Reactions that occur on the surface of a stimulus of an alternate phase are also heterogeneous. The collaborations between the homogeneous and heterogeneous reactions are extremely difficult and thus become a source of motivation, but it is still ambiguous.

The highly complex state of interaction occurs during these reactions. The rate of consumption and products of reactant within system (fluid and catalyst surface) is different for homogeneous/heterogeneous reactions. That situation intensifies the complexity of state of reaction. Initially, Merkin [24] inspected the laminar flow of viscous fluid with such type of reactions. Abbas et al. [25] studied the viscous fluid flow in existence of homogeneous and heterogeneous reactions and slip conditions. Hayat et al. [26] deliberated the flow of carbon nanotubes past a nonlinear stretchable sheet with variable thickness and heterogeneous/homogeneous. Recent development related to heterogeneous/homogeneous reactions can be seen via Refs. [27, 28, 29, 30, 31].

The main objective of present article is to explore the combined effect of mixed convection and axisymmetric stagnation point flow of Jeffrey fluid. Flow is caused by an inclined permeable stretching cylinder. The novelty of problem is to investigate the Cattaneo-Christov heat flux model for non-Newtonian fluid model with additional effects of homogeneous/heterogeneous reactions, mixed convection, stagnation point and thermal stratification. The novel non-Fourier heat flux model is employed with combined effects of homogeneous/heterogeneous reactions. Strong nonlinear ordinary differential system is attained by employing suitable transformations. Convergent series solutions of differential systems are obtained by HAM [32, 33, 34, 35, 36, 37, 38]. Currently some latest work has been cited (see refs [39, 40, 41, 42, 43]). Moreover, the skin friction coefficient and Nusselt number are discussed. Velocity, temperature and concentration profiles are also studied for different emerging parameters.

2. Model

Consider steady two-dimensional stagnation-point flow of an incompressible Jeffrey liquid over an inclined permeable stretching cylinder of radius R_c that makes an angle α_1 with vertical. Homogeneous/heterogeneous reactions is presented. Heat transfer phenomenon is analyzed with the Cattaneo-Christov heat flux theory. The problem is deliberated under cylindrical polar coordinates $(r, \theta, z)$with velocity components (u, v, w). The surface of inclined cylinder is being stretched with the velocity $U_w(z) = \frac{U_0 z}{L}$. The axisymmetric coordinate system is chosen in such a way that the z-axis is along the cylinder and r-axis is normal to the cylinder (see Fig. 1). The surface of the cylinder is maintained at variable temperature $T_w\left(= T_0 + \frac{D_1 z}{L}\right)$. The effect of external forces and pressure gradient is supposed to be negligible.

The homogeneous reactions are assumed to be of the cubic autocatalysis in form (Eq. 1)

$$\widehat{A} + \widehat{B} \rightarrow 3\widehat{B}, \quad rate = \widehat{k}_1 ab^2, \tag{1}$$

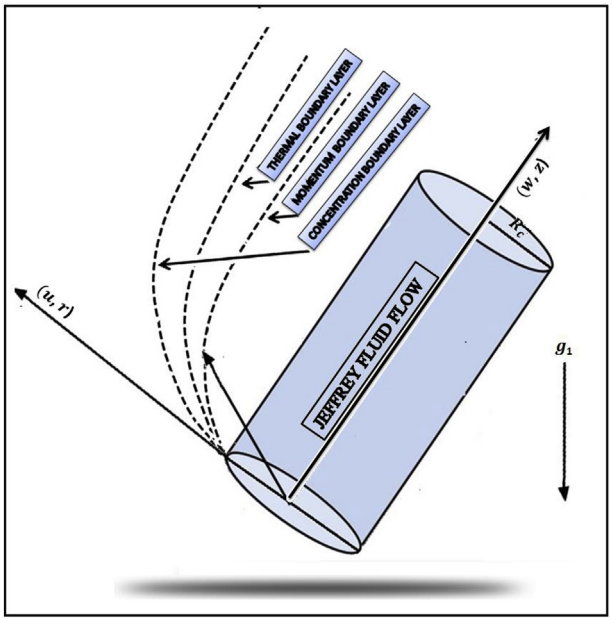

Fig. 1. Physical model.

Isothermal reaction of first order on catalyst surface is defined in Eq. (2)

$$\widehat{A} \rightarrow \widehat{B}, \quad rate = \widehat{k}_2 a, \tag{2}$$

where (a) and (b) symbolize the concentrations of the chemical species $\widehat{A}$ and $\widehat{B}$, while $(\widehat{k}_1, \widehat{k}_2)$ defines the rate constants. We also supposed that heat released during homogeneous/heterogeneous state of reaction is negligible. The constitutive equations for a Jeffrey fluid model are defined in Eqs. (3) and (4)

$$\tau = -PI + S \tag{3}$$

$$S = \frac{\mu}{(1+\xi_1)}\left[A_1 + \xi_2\left(\frac{\partial A_1}{\partial t} + V.\nabla\right)A_1\right] \tag{4}$$

where (μ) denotes dynamic viscosity, (ξ_1) for relaxation to retardation time ratio, (ξ_2) retardation time and $A_1 (= grad\, V + (grad\, V)^t)$ for first Rilvin-Erickson tensor respectively. This model comprises the features of viscous fluid and second grade fluid.

If $\xi_1 = \xi_2 = 0$, then problem characterize the viscous fluid model.
If $\xi_1 \neq 0$ *and* $\xi_2 = 0$, then problem represent the second-grade fluid.
If $\xi_1 \neq \xi_2 \neq 0$ then, problem signify Jeffrey fluid model.

The conservation laws after using the boundary layer approximations [44, 45, 46, 47, 48] and the above considered assumptions are given by Eqs. (5), (6), (7), (8), and (9)

$$\frac{\partial}{\partial r}(ru) + \frac{\partial}{\partial z}(rw) = 0, \tag{5}$$

$$\left.\begin{aligned} w\frac{\partial w}{\partial z} + u\frac{\partial w}{\partial r} = U_e(z)\frac{dU_e}{dz} + \frac{\nu_1}{(1+\xi_1)}\left(\frac{\partial^2 w}{\partial r^2} + \frac{1}{r}\frac{\partial w}{\partial r}\right) + g_1\beta_1(T - T_\infty)cos\alpha_1 \\ \frac{\nu_1\xi_2}{(1+\xi_1)}\left(u\frac{\partial^3 w}{\partial r^3} + \frac{\partial u}{\partial r}\frac{\partial^2 w}{\partial r^2} + w\frac{\partial^3 w}{\partial z \partial r^2} + \frac{\partial w}{\partial r}\frac{\partial^2 w}{\partial r \partial z} + \frac{1}{r}\left(u\frac{\partial^2 w}{\partial r^2} + w\frac{\partial^2 w}{\partial r \partial z}\right)\right), \end{aligned}\right\} \tag{6}$$

$$\rho_1 C_p\left(w\frac{\partial T}{\partial z}+u\frac{\partial T}{\partial r}\right)=\nabla.\boldsymbol{q}, \tag{7}$$

$$u\frac{\partial a}{\partial r}+w\frac{\partial a}{\partial z}=D_A\left(\frac{\partial^2 a}{\partial r^2}+\frac{1}{r}\frac{\partial a}{\partial r}\right)-\widehat{k}_1 ab^2, \tag{8}$$

$$u\frac{\partial b}{\partial r}+w\frac{\partial b}{\partial z}=D_B\left(\frac{\partial^2 b}{\partial r^2}+\frac{1}{r}\frac{\partial b}{\partial r}\right)-\widehat{k}_1 ab^2, \tag{9}$$

Here (ν_1), (β_1), (U_e) *and* (α_1)indicate the kinematic viscosity, mixed convection coefficient, free stream velocity and angle of inclination respectively. Moreover (L), (ρ_1), (C_p) *and* $(\boldsymbol{q})$ signify characteristic length, density, specific heat and heat flux respectively. Here D_A *and* D_B identify diffusion species coefficients.

In the past, heat transfer analysis has been performed by means of classical Fourier's law of heat conduction. Energy equation via Fourier's law is of parabolic type. It shows that the whole system is instantly affected by the initial disturbance. Mathematically, it is written in Eq. (10)

$$\mathbf{q}=-k\nabla \mathrm{T}, \tag{10}$$

where k represents thermal conductivity of fluid and negative sign indicates that heat flux moves from higher temperature region to lower one. Main drawback of his model is that initial disturbance is suddenly recognized by the medium under consideration. In practical life this could not be possible, so this is called "**paradox of heat conduction**". This issue has been controlled through the thermal relaxation time in the Fourier's law (see Cattaneo [13]). Mathematically, it is presented in Eq. (11)

$$\mathbf{q}+\xi_3\frac{\partial \mathbf{q}}{\partial t}=-k\nabla \mathrm{T}, \tag{11}$$

where ξ_3 represents the thermal relaxation time and new term $\left(i.e.\ \xi_3\frac{\partial \mathbf{q}}{\partial t}\right)$ involved above is identified as Thermal inertia. In 2009, Christov (see ref. [14]) improved the analysis of Cattaneo [13] by introducing thermal relaxation time and using Oldroyd's upper convected derivatives for the material-invariant formulation. Cattaneo-Christov heat flux [49, 50] is mentioned in Eq. (12)

$$\mathbf{q}+\xi_3\left[\frac{\partial \mathbf{q}}{\partial t}+\boldsymbol{V}.\nabla\mathbf{q}-\mathbf{q}.\nabla\boldsymbol{V}+(\nabla.\boldsymbol{V})\boldsymbol{q}\right]=-k\nabla \mathrm{T}, \tag{12}$$

It is mentioned that the Cattaneo–Christove model has some limitations i. e for $\xi_3=0$, Eq. (12) reduces to the classical Fourier law. Due to existence of thermal relaxation time factor $(\xi_3\neq 0)$, the paradox of heat conduction is rectified.

For steady and incompressible fluid situation one has (Eq. 13)

$$\mathbf{q}+\xi_3[\boldsymbol{V}.\nabla\mathbf{q}-\mathbf{q}.\nabla\boldsymbol{V}]=-k\nabla \mathrm{T}, \tag{13}$$

Elimination of heat flux $\mathbf{q}$ from Eqs. (7) and (13), we have

$$u\frac{\partial T}{\partial r}+w\frac{\partial T}{\partial z}+\xi_3\left(\begin{array}{c}u^2\frac{\partial^2 T}{\partial r^2}+w^2\frac{\partial^2 T}{\partial z^2}+\frac{\partial T}{\partial r}\left(w\frac{\partial u}{\partial z}+u\frac{\partial u}{\partial r}\right)+\\ \left(w\frac{\partial w}{\partial z}+u\frac{\partial w}{\partial r}\right)\frac{\partial T}{\partial z}+2wu\frac{\partial^2 w}{\partial r\partial z},\end{array}\right)$$
$$=\alpha_c\left(\frac{\partial^2 T}{\partial r^2}+\frac{1}{r}\frac{\partial T}{\partial r}\right), \tag{14}$$

here, $\alpha_c\left(=\frac{k}{\rho_1 C_p}\right)$ is the thermal diffusivity of the fluid.

The boundary conditions of the considered flow problem are given in Eq. (15)

$$\left.\begin{array}{l}\left.\begin{array}{lll}w=U_w=\frac{U_0 z}{L}, & u=V_1, & T=T_w=T_0+\frac{D_1 z}{L},\\ D_A\frac{\partial a}{\partial r}=\widehat{k}_2 a & D_B\frac{\partial b}{\partial r}=-\widehat{k}_2 a & \end{array}\right| \quad at\ r=R_c,\\ \left.\begin{array}{lll}w\to U_e(z)=\frac{U_\infty z}{L} & T\to\ T_\infty=T_0+\frac{D_2 z}{L}, & \\ a\to a_0, & b\to 0, & \end{array}\right| \quad when\ r\to\infty,\end{array}\right\} \tag{15}$$

By introducing the following dimensionless variables [51].

$$\left.\begin{array}{ll}\eta=\sqrt{\frac{U_0}{L\nu_1}}\left(\frac{r^2-R_c^2}{2R_c}\right), & u(\eta)=-\frac{R_c}{r}\sqrt{\frac{U_0}{\nu_1 L}}f(\eta)\\ w(\eta)=\frac{U_0 z}{L}f'(\eta), & \Theta(\eta)=\frac{T-T_\infty}{T_w-T_0},\\ a=a_0 g(\eta), & b=b_0 h(\eta),\end{array}\right| \tag{16}$$

The incompressibility condition is automatically satisfied and flow expressions [52, 53, 54] are given below (Eqs. (17), (18), (19), and (20))

$$\left.\begin{array}{l}(1+2\Lambda\eta)f'''+(1+\xi_1)\left(ff''-f'^2\right)+2\Lambda f''+\Lambda\beta_c(f'f''-3ff''')\\ +(1+2\Lambda\eta)\beta_c\left(f''^2-ff^{(4)}\right)+(1+\xi_1)A_c^2+\xi_m(1+\xi_1)\theta cos\alpha_1=0,\end{array}\right\} \tag{17}$$

$$\left.\begin{array}{l}(1+2\Lambda\eta)\theta''+2\Lambda\theta'-Pr(\widehat{S}_1+\theta')f'+Prf\theta'+\\ Pr\alpha_c\left((\widehat{S}_1+\theta')\left(ff''-f'^2\right)+ff'\theta'-f^2\theta''\right)=0,\end{array}\right\} \tag{18}$$

$$(1+2\Lambda\eta)g''+2\Lambda g'+Scfg'-ScK_m gh^2=0, \tag{19}$$

$$(1+2\Lambda\eta)h''+2\Lambda h'+\frac{Sc}{\delta}fh'-\frac{Sc}{\delta}K_m gh^2=0, \tag{20}$$

Transformed boundary conditions (Eq. (21)) are

$$\left.\begin{array}{lll}f'(0)=1, & f(0)=V_c, & \theta(0)=1-\widehat{S}_1,\\ g'(0)=K_t g(0), & \delta h'(0)=K_t g(0), & f'(\infty)\to A_c,\\ \theta(\infty)\to 0, & g(\infty)\to 1, & h(\infty)\to 0,\end{array}\right| \tag{21}$$

Here (Λ) characterizes curvature parameter, (β_c) Deborah number in form of retardation time, (A_c) velocity ratio, (K_m) strength of homogeneous reaction parameter, (K_t) strength of heterogeneous reaction parameter, (δ) mass diffusion ratio, (Sc) Schmidt number, (α_c) thermal relaxation factor and (Pr.) for Prandtl number respectively. The above-mentioned parameters are mathematically defined in Eq. (22).

$$\left.\begin{array}{lll}\Lambda=\sqrt{\frac{\nu_1 L}{U_0 R_c^2}}, & \beta_c=\frac{U_0\xi_2}{L}, & \alpha_c=\frac{U_0\xi_3}{L}\\ K_t=\frac{\widehat{k}_2}{D_A}\sqrt{\frac{\nu_1 L}{U_0}}, & Pr=\frac{\mu C_p}{k}, & A_c=\frac{U_\infty}{U_0},\\ K_m=\frac{\widehat{k}_1 a_0^2 L}{U_0}, & \delta_c=\frac{D_B}{D_A}, & Sc=\frac{\nu_1}{D_A}.\end{array}\right| \tag{22}$$

The size of $\widehat{A}$ and $\widehat{B}$ are considered to be comparable so that we further assume the equality of diffusion coefficients as a special case i.e., $D_A=D_B(\delta=1)$.Thus we have

$$g(\eta)+h(\eta)=0, \tag{23}$$

Invoking Eq. (23) into Eqs. (19) and (20), we get Eq. (24).

$$(1+2\Lambda\eta)g''+2\Lambda g'+Scfg'-ScK_cg(1-g)^2=0, \tag{24}$$

The local skin friction coefficient C_f (surface drag) and the local Nusselt number Nu_z (rate of heat transfer) are defined as follow (Eq. 25):

$$\left.\begin{aligned} C_f&=\frac{\tau_w}{\rho_1 U_w^2},\\ Nu_z&=\frac{zq_w}{k(T_w-T_0)}\end{aligned}\right\} \tag{25}$$

Shear stress (τ_w) and heat flux (q_w) are presented in Eqs. (26) and (27).

$$\tau_w=\frac{\mu_1}{(1+\xi_1)}\frac{\partial w}{\partial r}+\frac{\mu_1\xi_2}{(1+\xi_1)}\left(u\frac{\partial^2 w}{\partial r^2}+w\frac{\partial^2 w}{\partial r\partial z}\right)\Big|_{r=R_c}, \tag{26}$$

$$q_w=-k\frac{\partial T}{\partial r}\Big|_{r=R_c}, \tag{27}$$

Above physical quantities in dimensionless form are

$$\frac{1}{2}C_f(Re_z)^{1/2}=\frac{1}{(1+\xi_1)}[f''(0)-\beta_c(f(0)f'''(0)+\Lambda f(0)f''(0)-f'(0)f''(0))], \tag{28}$$

$$Nu_z(Re_z)^{-1/2}=-\theta'(0), \tag{29}$$

Where, $Re_z\left(=\frac{U_wL}{\nu_1}\right)$ is the local Reynolds number.

3. Methodology

Numerous methods are used for solving nonlinear equations. We have adopted homotopic technique (HAM) for our problem to get convergence solutions. Computations are performed with the aid of Mathematica software. Homotopy analysis method was first proposed by Liao [55] in 1992 which is used for the construction of series solution of highly nonlinear problems. In this method, we have great freedom for the selection of linear operators and initial guesses. The auxiliary linear operators and initial guesses are mentioned in Eqs. (30) and (31)

$$\left.\begin{aligned} f_o(\eta)&=1+V_c+A_c(\eta-1)+(A_c-1)exp[-\eta]\\ \theta_o(\eta)&=(1-\widehat{S}_1)exp[-\eta]\\ g_o(\eta)&=1-\frac{1}{2}exp[-K_t\eta]\end{aligned}\right. \tag{30}$$

$$\widehat{\pounds}_f[f]=f'''-f',\quad \widehat{\pounds}_\theta[\theta]=\theta''-\theta,\quad \widehat{\pounds}_g[g]=g''-g \tag{31}$$

The above mentioned operators $\widehat{\pounds}_f$, $\widehat{\pounds}_\theta$ and $\widehat{\pounds}_g$ satisfy the following properties Eq. (32)

$$\left.\begin{aligned} &\widehat{\pounds}_f[\dot{N}_2exp(-\eta)+\dot{N}_1+\dot{N}_3exp(\eta)]=0,\ \widehat{\pounds}_\theta[\dot{N}_4exp(-\eta)+\dot{N}_5exp(\eta)]=0,\ \widehat{\pounds}_g[\dot{N}_6exp(-\eta)+\dot{N}_7exp(\eta)]=0.\end{aligned}\right. \tag{32}$$

where constants $\dot{N}_i$ notify the arbitrary constants for i= (1–7).

3.1. Zeroth-order equations

The problems statements at this order (Eqs. (33) and (34)) are

$$\left.\begin{aligned} (1-q)\widehat{\pounds}_f[\widehat{f}(\eta;q)-f_o(\eta)]&=qh_fN_f[\widehat{f}(\eta;q);\widehat{\theta}(\eta;q);\widehat{g}(\eta;q)]\\ (1-q)\widehat{\pounds}_\theta[\widehat{\theta}(\eta;q)-\theta_o(\eta)]&=qh_\theta N_\theta[\widehat{f}(\eta;q);\widehat{\theta}(\eta;q);\widehat{g}(\eta;q)]\\ (1-q)\widehat{\pounds}_g[\widehat{g}(\eta;q)-g_o(\eta)]&=qh_gN_g[\widehat{f}(\eta;q);\widehat{\theta}(\eta;q);\widehat{g}(\eta;q)]\end{aligned}\right. \tag{33}$$

$$\left.\begin{aligned} &\widehat{f}'(0;q)=1, && \widehat{f}(0;q)=V_c, && \widehat{\theta}(0;q)=1-\widehat{S}_1,\\ &\widehat{g}'(0;q)=K_t\widehat{g}(0;q), && \widehat{f}'(\infty;q)=A_c, && \widehat{\theta}(\infty;q)=0,\\ & && \widehat{g}(\infty;q)=1, &&\end{aligned}\right| \tag{34}$$

where $N_{\hat{f}}$, N_{θ} *and* N_g are expressed in Eqs. (35), (36), and (37)

$$\left.\begin{aligned} N_{\hat{f}}[\widehat{f}(\eta;q);\widehat{\theta}(\eta;q);\widehat{g}(\eta;q)]&=(1+2\Lambda\eta)\left(\frac{\partial^3\widehat{f}(\eta;q)}{\partial\eta^3}+\beta_c\left(\left(\frac{\partial^2\widehat{f}(\eta;q)}{\partial\eta^2}\right)^2-\widehat{f}(\eta;q)\frac{\partial^4\widehat{f}(\eta;q)}{\partial\eta^4}\right)\right)\\ &+(1+\xi_1)\left(\widehat{f}(\eta;q)\frac{\partial^2\widehat{f}(\eta;q)}{\partial\eta^2}-\frac{\partial\widehat{f}(\eta;q)}{\partial\eta}\frac{\partial\widehat{f}(\eta;q)}{\partial\eta}+A_c^2+\xi_m\widehat{\theta}(\eta;q)cos\alpha_1\right)+\\ &2\Lambda\frac{\partial^2\widehat{f}(\eta;q)}{\partial\eta^2}+\Lambda\beta_c\left(\frac{\partial\widehat{f}(\eta;q)}{\partial\eta}\frac{\partial^2\widehat{f}(\eta;q)}{\partial\eta^2}-3\widehat{f}(\eta;q)\frac{\partial^3\widehat{f}(\eta;q)}{\partial\eta^3}\right),\end{aligned}\right\} \tag{35}$$

$$\left.\begin{aligned} N_\theta[\widehat{f}(\eta;q);\widehat{\theta}(\eta;q);\widehat{g}(\eta;q)]&=(1+2\Lambda\eta)\frac{\partial^2\widehat{\theta}(\eta;q)}{\partial\eta^2}+2\Lambda\frac{\partial\widehat{\theta}(\eta;q)}{\partial\eta}\\ &-Pr\left(\frac{\partial\widehat{\theta}(\eta;q)}{\partial\eta}\frac{\partial\widehat{f}(\eta;q)}{\partial\eta}+\widehat{S}_1\frac{\partial\widehat{f}(\eta;q)}{\partial\eta}-\widehat{f}(\eta;q)\frac{\partial\widehat{\theta}(\eta;q)}{\partial\eta}\right)+\\ &Pr\alpha_c\left((\widehat{\theta}(\eta;q)+\widehat{S}_1)\widehat{f}(\eta;q)\frac{\partial^2\widehat{f}(\eta;q)}{\partial\eta^2}-\left(\frac{\partial\widehat{f}(\eta;q)}{\partial\eta}\right)^2\right.\\ &\left.+\widehat{f}(\eta;q)\frac{\partial\widehat{f}(\eta;q)}{\partial\eta}\frac{\partial\widehat{\theta}(\eta;q)}{\partial\eta}-(\widehat{f}(\eta;q))^2\frac{\partial^2\widehat{\theta}(\eta;q)}{\partial\eta^2}\right)\end{aligned}\right\} \tag{36}$$

$$\left.\begin{aligned} N_g[\widehat{f}(\eta;q);\widehat{\theta}(\eta;q);\widehat{g}(\eta;q)]&=(1+2\Lambda\eta)\frac{\partial^2\widehat{g}(\eta;q)}{\partial\eta^2}+2\Lambda\frac{\partial\widehat{g}(\eta;q)}{\partial\eta}\\ &+Sc\widehat{f}(\eta;q)\frac{\partial\widehat{g}(\eta;q)}{\partial\eta}-ScK_c\widehat{g}(\eta;q)(1-\widehat{g}(\eta;q))^2\end{aligned}\right\} \tag{37}$$

3.2. Deformation equations ($\mathbf{m^{th}-order}$)

The m^{th} order system (Eqs. (38) and (39)) is

$$\left.\begin{aligned}&\widehat{\pounds}_f[f_m(\eta)-\underline{\chi}_m f_{m-1}(\eta)]=h_f R_m^f(\eta),\\&\widehat{\pounds}_\theta[\theta_m(\eta)-\underline{\chi}_m \theta_{m-1}(\eta)]=h_\theta R_m^\theta(\eta)\\&\widehat{\pounds}_g[g_m(\eta)-\underline{\chi}_m g_{m-1}(\eta)]=h_g R_m^g(\eta)\end{aligned}\right\} \tag{38}$$

with

$$\left.\begin{aligned}&f(0)=0, \quad f'(0)=0, \quad \theta(0)=0,\\&g'(0)=0, \quad f'(\infty)=0, \quad \theta(\infty)=0,\\&\qquad\quad g(\infty)=0,\end{aligned}\right| \tag{39}$$

where $R_m^f(\eta)$, $R_m^\theta(\eta)$ and $R_m^g(\eta)$ are marked in Eqs. (40), (41), and (42)

$$\left.\begin{aligned}&R_m^f(\eta)=(1+2\Lambda\eta)\left(f'''_{m-1}+\beta_c\sum_{k=0}^{m-1}\left(f''_{m-1-k}f''_k-f_{m-1-k}f_k^{iv}\right)\right)+\\&(1+\xi_1)\left(\sum_{k=0}^{m-1}\left(f_{m-1-k}f''_k-f'_{m-1-k}f'_k+A_c^2(1-\underline{\chi}_m)\right)+\xi_m\theta_{m-1}cos\alpha_1\right)\\&+\Lambda\beta_c\sum_{k=0}^{m-1}\left(f'_{m-1-k}f''_k-3f_{m-1-k}f'''_k+2f''_{m-1}\right),\end{aligned}\right\} \tag{40}$$

$$\left.\begin{aligned}&R_m^\theta(\eta)=(1+2\Lambda\eta)\theta''_{m-1}+2\Lambda\theta'_{m-1}-Pr\widehat{S}_1f'_{m-1}-\\&Pr\sum_{k=0}^{m-1}\left(\theta_{m-1-k}f'_k-f_{m-1-k}\theta'_k+\widehat{S}_1\alpha_c\left(f'_{m-1-k}f'_k-f_{m-1-k}f''_k\right)\right)\\&+Pr\alpha_c\sum_{k=0}^{m-1}\left(\begin{aligned}&\theta_{m-1-k}\sum_{l=0}^{k}f_{k-l}f''_l-\theta_{m-1-k}\sum_{l=0}^{k}f'_{k-l}f'_l\\&+f_{m-1-k}\sum_{l=0}^{k}f'_{k-l}\theta'_l-f_{m-1-k}\sum_{l=0}^{k}f_{k-l}\theta''_l\end{aligned}\right),\end{aligned}\right\} \tag{41}$$

$$\left.\begin{aligned}&R_m^g(\eta)=(1+2\Lambda\eta)g''_{m-1}+2\Lambda g'_{m-1}-ScK_cg_{m-1}+\\&Sc\sum_{k=0}^{m}(f_{m-1-k}+2K_cg_{m-1-k})g_k-K_cg_{m-1-k}\sum_{l=0}^{k}g_{k-l}g_l,\end{aligned}\right\} \tag{42}$$

$$\underline{\chi}_m=\left\{\begin{matrix}0 & m\le 1\\1 & m>1\end{matrix}\right|. \tag{43}$$

For $\dot{q}=0$ and $\dot{q}=1$we have (Eq. (44))

$$\left.\begin{aligned}&\widehat{f}(\eta;0)=f_o(\eta), \quad \widehat{\theta}(\eta;0)=\theta_o(\eta), \quad \widehat{g}(\eta;0)=g_o(\eta),\\&\widehat{f}(\eta;1)=f(\eta), \quad \widehat{\theta}(\eta;1)=\theta(\eta), \quad \widehat{g}(\eta;1)=g(\eta),\end{aligned}\right\} \tag{44}$$

According to Taylor's series expansion, we have Eqs. (45), (46), and (47)

$$\left.\begin{aligned}&\widehat{f}(\eta;q)=f_o(\eta)+\sum_{m=1}^{\infty}f_m(\eta)q^m\\&f_m(\eta)=\frac{1}{m!}\frac{\partial^m}{\partial q^m}\widehat{f}_m(\eta;q)\Big|_{q=0},\end{aligned}\right. \tag{45}$$

$$\left.\begin{aligned}&\widehat{\theta}(\eta;q)=\theta_o(\eta)+\sum_{m=1}^{\infty}\theta_m(\eta)q^m\\&\theta_m(\eta)=\frac{1}{m!}\frac{\partial^m}{\partial q^m}\widehat{\theta}_m(\eta;q)\Big|_{q=0},\end{aligned}\right. \tag{46}$$

$$\left.\begin{aligned}&\widehat{g}(\eta;q)=g_o(\eta)+\sum_{m=1}^{\infty}g_m(\eta)q^m\\&g_m(\eta)=\frac{1}{m!}\frac{\partial^m}{\partial q^m}\widehat{g}_m(\eta;q)\Big|_{q=0},\end{aligned}\right. \tag{47}$$

The general solution $(f_m(\eta),\ \theta_m(\eta),\ g_m(\eta))$in the form of special solutions $(\widehat{f}(\eta),\widehat{\theta}(\eta),\widehat{g}(\eta))$are written in Eqs. (48), (49), and (50)

$$f_m(\eta)=\widehat{f}(\eta)+\dot{N}_1+\dot{N}_2exp(-\eta)+\dot{N}_3exp(\eta), \tag{48}$$

$$\theta_m(\eta)=\widehat{\theta}(\eta)+\dot{N}_4exp(-\eta)+\dot{N}_5exp(\eta), \tag{49}$$

$$g_m(\eta)=\widehat{g}(\eta)+\dot{N}_6exp(-\eta)+\dot{N}_7exp(\eta), \tag{50}$$

in which constants $\dot{N}_i$ Eq. (51) are defined as

$$\dot{N}_1=-\widehat{f}'_m(0)-\widehat{f}_m(0), \qquad \dot{N}_2=\widehat{f}'_m(0),\ \dot{N}_4=-\widehat{\theta}_m(0),\dot{N}_6=\frac{1}{1+K_t}\widehat{g}'_m(0)-\frac{1}{1+K_t}\widehat{g}_m(0),\dot{N}_3=0, \qquad \dot{N}_5=\dot{N}_7=0, \tag{51}$$

4. Analysis

HAM technique provides great freedom to control rate of convergence of series solution by auxiliary parameters. To decide about convergence criteria after utilizing HAM we need accurate range of auxiliary parameters when h-curves are parallel to the horizontal axis. For this purpose, values of auxiliary parameters h_f, h_θ and h_g are selected from relevant range of plotted h-curves at 25^{th} iteration. Fig. 2 portrays the acceptable ranges of auxiliary parameters h_f, h_θ and h_g as $(-1.3\le h_f\le -0.4)$, $(-1.5\le h_\theta\le -0.5)$ and $(-1.2\le h_g\le -0.4)$. In this study, numerical computations are restricted thoroughly with practical range of non-dimensional parameters [56] as $(0.2\le\Lambda\le 0.8)$, $(0.1\le\xi_m\le 0.5)$, $(0.4\le\xi_1\le 1.5)$, $(0.2\le\beta_c\le 0.6)$, $(0.1\le\alpha_c\le 0.5)$, $(0.2\le\widehat{S}_1\le 0.6)$, $(0.1\le K_t\le 0.5)$, $(0.5\le Pr\le 2.5)$, $(0.1\le K_m\le 0.5)$ and $(0.1\le V_c\le 0.4)$. Table 1 is computed to present the convergence analysis of homotopic expressions. It is inspected that enough for 35^{th}order of approximations for momentum, energy and concentration equations. Table 2 is built to validate the present consequences with previously published results by Acharya [57], Khan and Pop [58] and Hsiao [59]. This table shows the great agreement with previous literature.

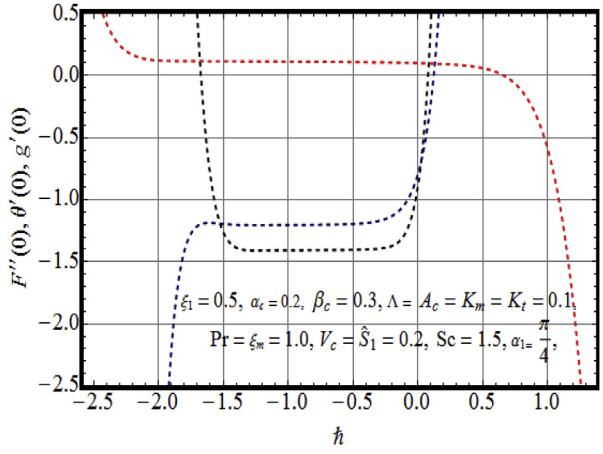

Fig. 2. $h-$ curves of $f''(0)$, $\theta'(0)$ *and* $g'(0)$.

Table 1
HAM convergence analysis when $\xi_1 = 0.5$, $\beta_c = 0.3$, $\alpha_c = 0.2$, $K_m = K_t = 0.1$, $\xi_m = Pr = 1.0$, $S_1 = 0.2$, $Sc = 1.5$, $V_c = 0.2$.

Approximation order	$f''(0)$	$\theta'(0)$	$g'(0)$
1	0.8587	0.6985	0.1382
7	0.8524	0.7322	0.1345
14	0.8554	0.7524	0.1360
20	0.8582	0.7959	0.1371
25	0.8607	0.7934	0.1450
30	0.8612	0.7668	0.1429
35	0.8624	0.7743	0.1408
40	0.8624	0.7743	0.1408
46	0.8624	0.7743	0.1408

Table 2
Numerical comparison of $-\theta(0)$ when $\Lambda = \widehat{\beta}_t = \widehat{\beta}_c = \xi_1 = A_c = \xi_m = \beta_c = \widehat{S}_1 = K_m = 0$ and $Pr = 5$.

α_c	Acharya et al. [57]	Khan and Pop [58]	Hsiao et al. [59]	Present (HAM)
0.1	0.9524	0.9524	0.952432	1.00124
0.2	0.6932	0.6932	0.693211	0.69582
0.3	0.5201	0.5201	0.520147	0.51596
0.4	0.4026	0.4026	0.402631	0.40236
0.5	0.3211	0.3211	0.321149	0.32340

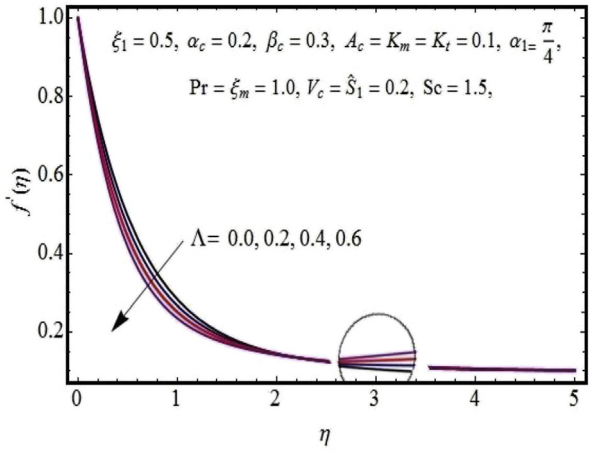

Fig. 3. Impact of Λ on $f'(\eta)$.

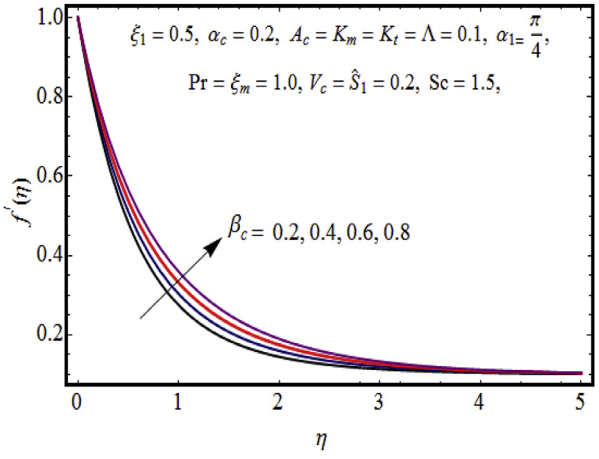

Fig. 4. Impact of β_c on $f'(\eta)$.

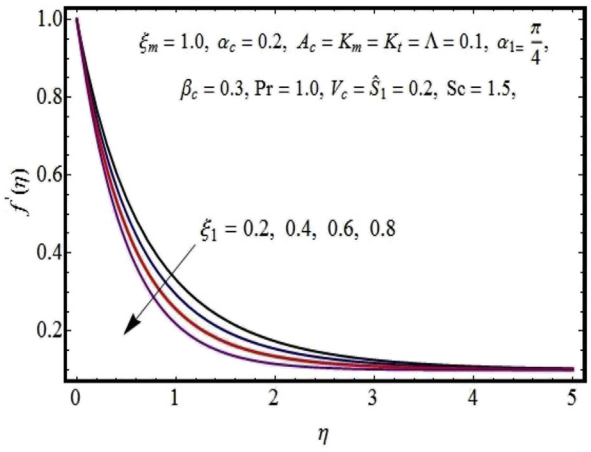

Fig. 5. Impact of ξ_1 on $f'(\eta)$.

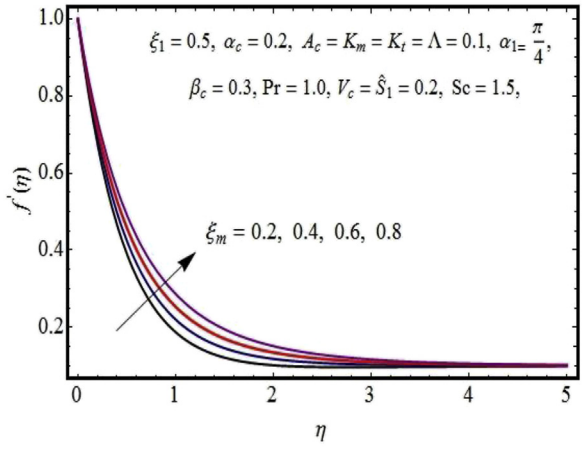

Fig. 6. Impact of ξ_m on $f'(\eta)$.

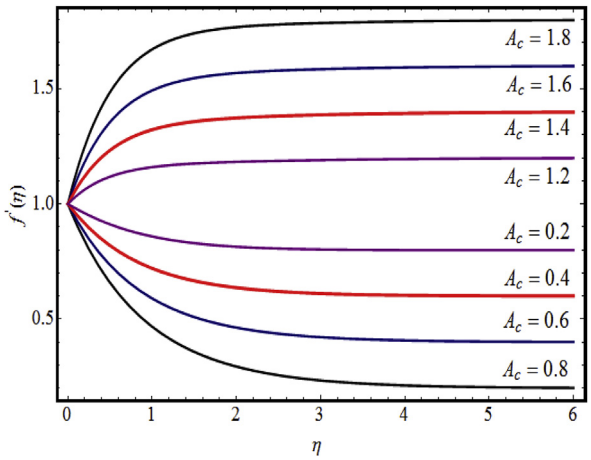

Fig. 7. Impact of A_c on $f'(\eta)$.

5. Results & discussion

The graphical analysis of parameters like curvature parameter (Λ), Deborah number (β_c), velocities ratio parameter (A_c), strength of homogeneous reaction parameter (K_m), strength of heterogeneous reaction parameter (K_t), mass diffusion ratio (δ_c), Schmidt number (Sc), thermal relaxation parameter (α_c), Prandtl number (Pr), fluid parameter (ξ_1),

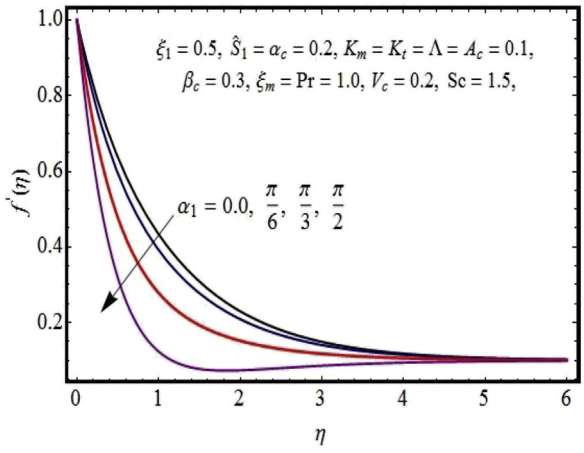

Fig. 8. Impact of α_1 on $f'(\eta)$.

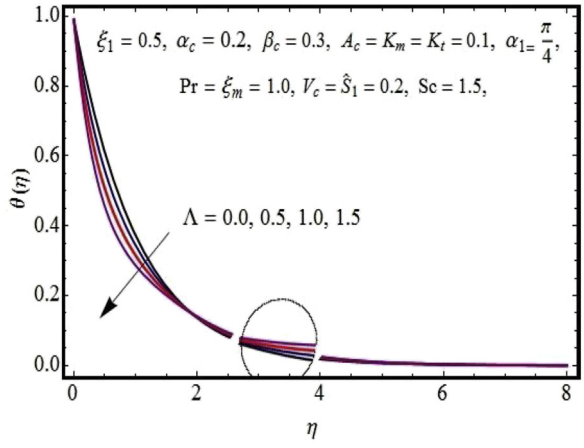

Fig. 9. Impact of Λ on $\theta(\eta)$.

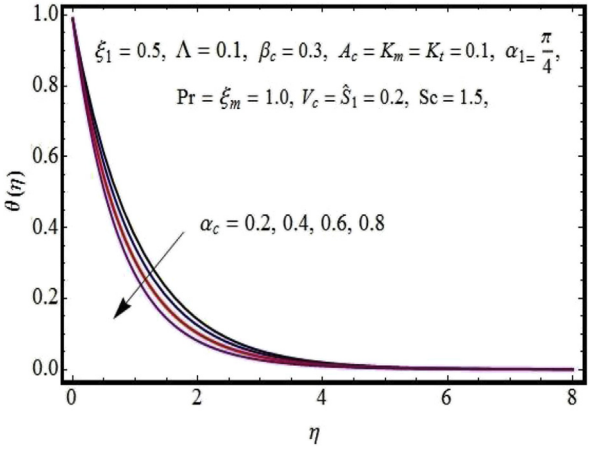

Fig. 10. Impact of α_c on $\theta(\eta)$.

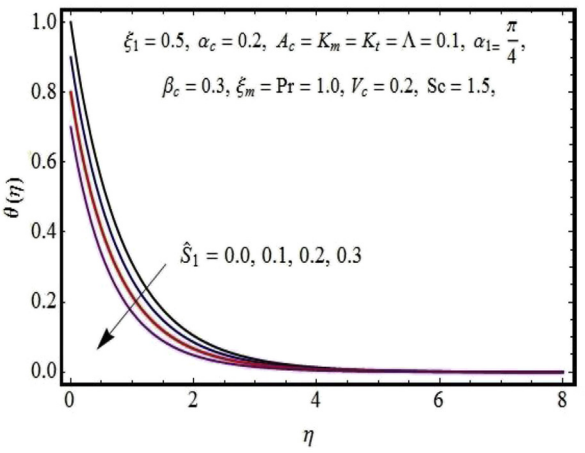

Fig. 11. Impact of S_1 on $\theta(\eta)$.

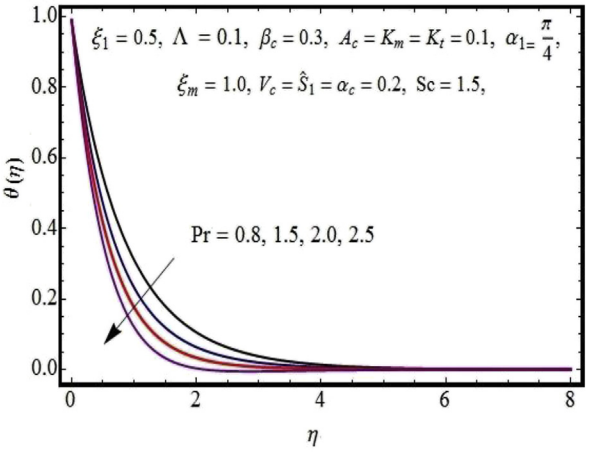

Fig. 12. Impact of Pr on $\theta(\eta)$.

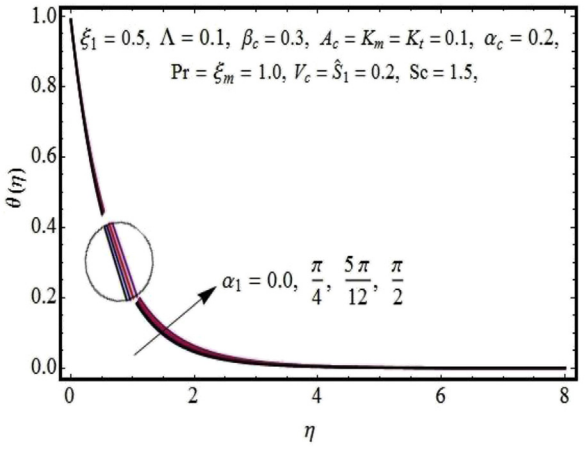

Fig. 13. Impact of α_1 on $\theta(\eta)$.

mixed convection parameter (ξ_m) and thermal stratification parameter (S_1) on velocity $f'(\eta)$, temperature $\theta(\eta)$ and concentration $g(\eta)$ is displayed in Figs. 3, 4, 5, 6, 7, 8, 9, 10, 11, 12, 13, 14, 15, and 16. In Fig. 3 role of curvature parameter (Λ) on $f'(\eta)$ is demonstrated. For higher value of curvature parameter (Λ), the velocity curve declines near the surface of cylinder and enhances away from it. Physically, increase of curvature parameter (Λ) yields the decrease in radius of cylinder that causes low resistance in flow field. As a result $f'(\eta)$ shows increasing behavior far away from the surface of cylinder. Consequence of Deborah number (β_c) on $f'(\eta)$ is illustrated via Fig. 4. The velocity $f'(\eta)$ profile and related momentum boundary layer thickness are amplified with the rise of Deborah number (β_c). In fact, increase of parameter (β_c) corresponds to the intensify the elasticity of fluid material. That is accountable for

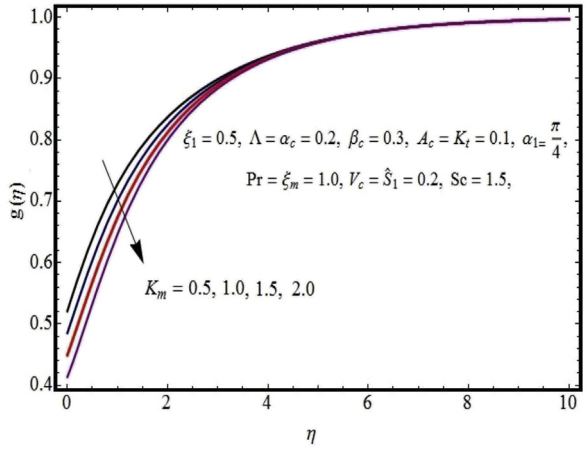

Fig. 14. Impact of K_m on $g(\eta)$.

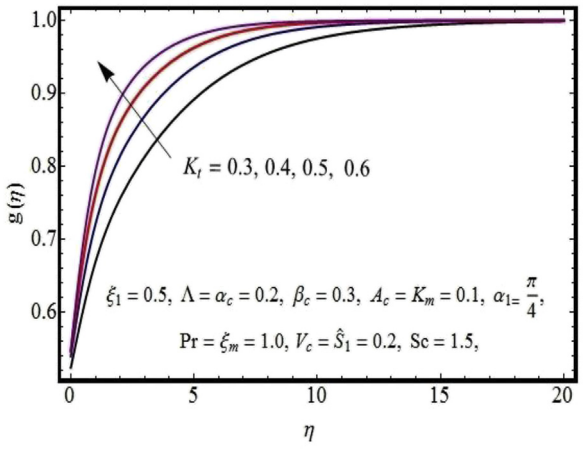

Fig. 15. Impact of K_t on $g(\eta)$.

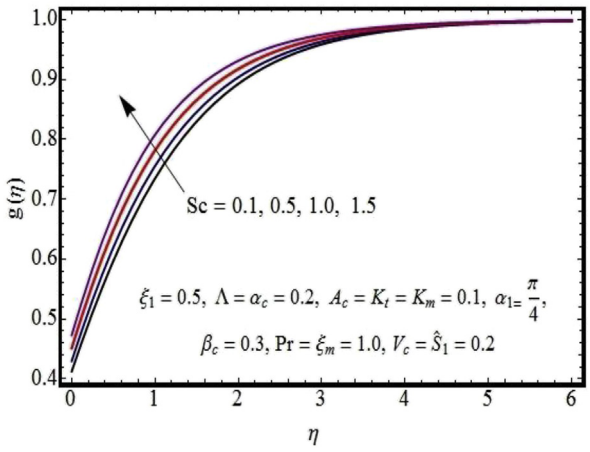

Fig. 16. Impact of Sc on $g(\eta)$.

increase in velocity profile $f'(\eta)$. Fig. 5 emphasis on the impact of fluid parameter (ξ_1) on velocity profile $f'(\eta)$. As expected, the velocity profile $f'(\eta)$ declines with the higher values of (ξ_1). Since (ξ_1) being ratio of relaxation to retardation time produces resistance to the fluid flow that eventually diminishes the velocity $f'(\eta)$. Noticeable characteristics of mixed convection parameter (ξ_m) are shown in Fig. 6. Physically increase of (ξ_m) is responsible to enhance the buoyancy forces. That results in enhancement of velocity $f'(\eta)$. Fig. 7 is revealed to study the features of velocities ratio parameter (A_c) on velocity $f'(\eta)$. It is observed from figure that velocity profile upsurge for both cases $A_c > 1$ and $A_c < 1$. The increase of (A_c) upsurges free stream velocity that eventually result in the improvement of $f'(\eta)$. This developing behavior of $f'(\eta)$ remained same when either free stream velocity dominates or followed. Thickness of boundary layer has reverse effects. Impact of angle of inclination (α_1) on velocity distribution is displayed in Fig. 8. The decaying nature of velocity field is observed for greater value of (α_1). Since, impact of gravity force decreases for higher altitude. That causes reduction in velocity profile. Fig. 9 depicts behavior of curvature parameter (Λ) on temperature $\theta(\eta)$. It is evident that temperature $\theta(\eta)$ declines near surface of cylinder and it enhances away from it for greater values of (Λ). Variation of thermal relaxation parameter (α_c) on temperature $\theta(\eta)$ is shown in Fig. 10. Increase in (α_c) leads to decrease in both temperature $\theta(\eta)$ and thermal boundary layer thickness. Physically, for higher estimation of (α_c) fluid particle required more time to transfer heat to its adjacent particles. As a result, temperature curve decreases for greater (α_c). In Fig. 11, variation of temperature distribution $\theta(\eta)$ against thermal stratification parameter (S_1) is captured. In fact, temperature difference $(T_w - T_\infty)$ gradually decreases for higher approximation of (S_1)that ultimately declines the temperature curve. The temperature and thermal boundary layer thickness are decreased significantly for greater values of Prandtl number (Pr)(see Fig. 12). Since, Prandtl number is the ratio of momentum to thermal diffusivities. For higher Prandtl number momentum diffusivity enhances while thermal diffusivity diminishes. Here weaker thermal diffusivity dominant over the stronger momentum diffusivity. Therefore, temperature profile reduces. Fig. 13 is plotted to study the impact of (α_1) on temperature profile $\theta(\eta)$. Enhancing behavior of temperature is observed for greater approximation of (α_1). Since, gravity impact decreases with inclination that becomes a source of declining in heat transfer rate. Hence, temperature field $\theta(\eta)$ increases. Variation of homogeneous reaction $(K_m)$and heterogeneous reaction parameters $(K_t)$for concentration distribution $g(\eta)$ is shown in Figs. 14 and 15. Conflicting behavior of both parameters is noticed for concentration and associated layer thickness. Since reactants are consumed during homogeneous reaction and consequently fluid concentration denigrates which is apparently seen from this figure (see Fig. 14). It is noticed that the concentration boundary layer thickness upsurges with increasing (K_t) which agrees with the common physical behavior of the homogeneous and heterogeneous reactions parameters. Variation of concentration profile $g(\eta)$ against Schmidt number (Sc) is displayed in Fig. 16. For greater values of (Sc), the concentration profile $g(\eta)$ is found to be growing. In fact, the Schmidt number is defined as the ratio of momentum diffusivity to mass diffusivity. Therefore, higher values of the Schmidt number correspond to reduce the mass diffusivity. The role of

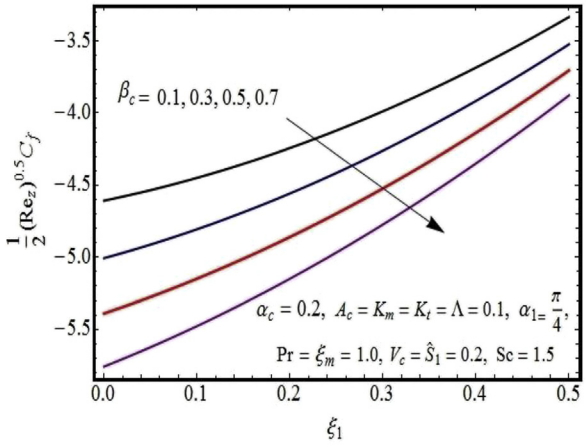

Fig. 17. Impact of β_c on $\frac{1}{2}(Re)^{0.5}C_f$.

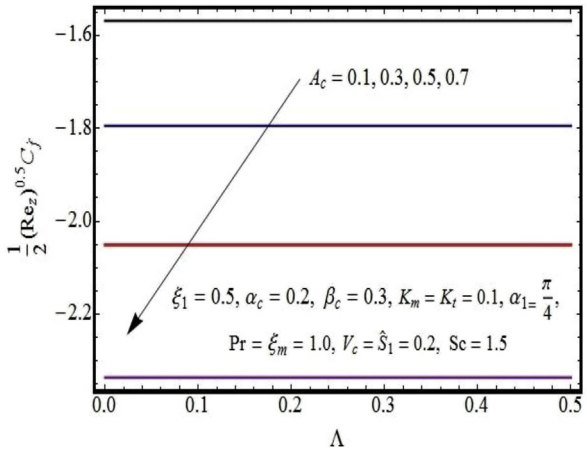

Fig. 18. Impact of A_c on $\frac{1}{2}(Re)^{0.5}C_f$.

skin friction coefficient C_f, for emerging parameters (β_c) and (A_c) are presented in Figs. 17 and 18. The dwindling influence of skin friction coefficient is observed for both (β_c) and (A_c).

6. Conclusions

In this study we analyze the homogeneous/heterogeneous reactions for Jeffery fluid model induced by an inclined stretching cylinder. Heat transfer analysis has been accomplished via Cattaneo-Christove heat flux model. Resulting equations have been transformed into dimensionless ODEs and solved via homotopic technique. Based on the entire study following conclusions can be figure out:

- ❖ Higher values of Deborah number result in the enhancement of velocity distribution.
- ❖ There is a direct relation of curvature parameter (Λ) with velocity and temperature profiles
- ❖ Velocity profile enhances with greater values of velocity ratio parameter (A_c) while it declines with fluid parameter (ξ_1).
- ❖ Effects of homogeneous $(K_m)$and heterogeneous (K_t) reaction parameters on the concentration profile are quite opposite.
- ❖ Temperature distribution reduces for higher approximation of Prandtl number (Pr) and thermal stratification parameter.

Declarations

Author contribution statement

M. Ijaz: Conceived and designed the experiments; Analyzed and interpreted the data; Contributed reagents, materials, analysis tools or data; Wrote the paper.

M. Ayub: Conceived and designed the experiments; Performed the experiments; Contributed reagents, materials, analysis tools or data.

Funding statement

This research did not receive any specific grant from funding agencies in the public, commercial, or not-for-profit sectors.

Competing interest statement

The authors declare no conflict of interest.

Additional information

No additional information is available for this paper.

References

[1] T. Hayat, A. Alsaedi, S.A. Shehzad, Three- dimensional flow of Jeffrey fluid with convective surface boundary conditions, Int. J. Heat Mass Transf. 55 (2012) 3971–3976.
[2] T. Hayat, M.I. Khan, M. Farooq, A. Alsaedi, Thermally stratified stretching flow with Cattaneo-Christov heat flux, Int. J. Heat Mass Transf. 106 (2017) 289–294.
[3] K.L. Hsiao, Stagnation electrical MHD nanofluid mixed convection with slip boundary on a stretching sheet, Appl. Therm. Eng. 98 (2016) 850–861.
[4] T. Hayat, S. Qayyum, S.A. Shehzad, A. Alsaedi, Simultaneous effects of heat generation/absorption and thermal radiation in magneto-hydrodynamics (MHD) flow of Maxwell nanofluid towards a stretched surface, Results Phys. 7 (2017) 562–573.
[5] F. Lanza, E. Parnisari, Influence of film formation and its composition on the leaching of borosilicate glasses, Nucl. Chem. Waste Manag. 2 (1981) 131–137.
[6] T. Hayat, S.A. Shehzad, M. Qasim, S. Obaidat, Radiative flow of Jeffrey fluid in a porous medium with power law heat flux and heat source, Nucl. Eng. Des. 243 (2012) 15–19.
[7] T. Hussain, S.A. Shehzad, T. Hayat, A. Alsaedi, Radiative hydromagnetic flow of Jeffrey nanofluid by an exponentially stretching sheet, PLoS One 9 (2014) 103719.
[8] T. Hayat, S. Qayyum, M. Imtiaz, A. Alsaedi, Impact of Cattaneo-Christov heat flux in Jeffrey fluid flow with homogeneous-heterogeneous reactions, PLoS One 11 (2016), 0148662.
[9] D. Tripathi, N. Ali, T. Hayat, M.K. Chaube, A.A. Hendi, Peristaltic flow of MHD Jeffrey fluid through finite length cylindrical tube, Appl. Math. Mech. 32 (2011) 1231–1244.
[10] G.B. Reddy, S. Sreenadh, R.H. Reddy, A. Kavitha, Flow of a Jeffrey fluid between torsionally oscillating disks, Ain. Shams Eng. J. 6 (2015) 355–362.
[11] M.A.A. Hamad, S.M.A. Gaied, W.A. Khan, Thermal jump effects on boundary layer flow of a Jeffrey fluid near the stagnation point on a stretching/shrinking sheet with variable thermal conductivity, J. Fluids 2013 (2013) 749271.
[12] J.B.J. Fourier, Théorie Analytique De La Chaleur, Paris, 1822.
[13] C. Cattaneo, Some aspects of diffusion theory, Atti Semin. Mat Fis Univ. Modena Reggio Emilia 3 (1948) 83–101.
[14] C.I. Christov, On frame indifferent formulation of the Maxwell-Cattaneo model of finite-speed heat conduction, Mech. Res. Commun. 39 (2009) 481–486.
[15] M. Ciarletta, B. Straughan, Uniqueness and structural stability for the Cattaneo-Christov equations, Mech. Res. Commun. 37 (2010) 445–447.
[16] S.A.M. Haddad, Thermal instability in Brinkman porous media with Cattaneo-Christov heat flux, Int. J. Heat Mass Transf. 68 (2014) 659–668.
[17] U. Ali, K.U. Rehman, M.Y. Malik, The Influence of MHD and Heat Generation/absorption in a Newtonian Flow Field Manifested with Cattaneo-Christov Heat Flux Model, 2019. https://iopscience.iop.org/article/10.1088/1402-4896/ab11ff/pdf.
[18] S.A.M. Mehryan, Mikhail A. Sheremet, M. Soltani, Mohsen Izadi, Natural convection of magnetic hybrid nanofluid inside a doubleporous medium using two-equation energy model, J. Mol. Liq. (2018).
[19] A. Tahmasebi, M. Mahdavi, M. Ghalambaz, Local thermal nonequilibrium conjugate natural convection heat transfer of nanofluids in a cavity partially filled with porous media using Buongiorno's model, Numer. Heat Transf. Appls., Part A: Appl 73 (2018) 254–276.
[20] M. Zubair, M. Ijaz, T. Abbas, A. Riaz, Analysis of modified Fourier law in flow of ferromagnetic Powell-Eyring fluid considering two equal magnetic dipoles, Can. J. Phys. 97 (7) (2019) 772–776.
[21] M. Ijaz, M. Ayub, Simulation of magnetic dipole and dual stratification in radiative flow of ferromagnetic Maxwell fluid, Heliyon 5 (2019), e01465.
[22] S. Nadeem, N. Muhammad, Impact of stratification and Cattaneo-Christov heat flux in the flow saturated with porous medium, J. Mol. Liq. 224 (2016) 423–430.
[23] M. Bibi, M.Y. Malik, A. Zeeshan, Numerical analysis of unsteady magneto-biphase Williamson fluid flow with time dependent magnetic field, Commun. Theor. Phys. 71 (2019) 143–151.
[24] J.H. Merkin, A model for isothermal homogeneous-heterogeneous reactions in boundary layer flow, Math. Comput. Model. 24 (1996) 125–136.
[25] Z. Abbas, M. Sheikh, I. Pop, Stagnation-point flow of a hydromagnetic viscous fluid over stretching/shrinking sheet with generalized slip condition in the presence of homogeneous heterogeneous reactions, J. Taiwaan Inst. Chem. Eng. 55 (2015) 69–75.
[26] T. Hayat, Z. Hussain, T. Muhammad, A. Alsaedi, Effects of homogeneous and heterogeneous reactions in flow of nanofluids over a nonlinear stretching surface with variable surface thickness, J. Mol. Liq. 221 (2016) 1121–1127.
[27] M.I. Khan, M. Waqas, T. Hayat, A. Alsaedi, A comparative study of Casson fluid with homogeneous-heterogeneous reactions, J. Colloid Interface Sci. 498 (2017) 85–90.
[28] T. Hayat, F. Haider, T. Muhammad, A. Alsaedi, Darcy-Forchheimer flow with Cattaneo-Christov heat flux and homogeneous-heterogeneous reactions, PLoS One 12 (2017), 0174938.
[29] S. Nadeem, M.Y. Malik, Nadeem Abbas, Heat transfer of three dimensional micropolar fluids on Riga plate, Can. J. Phys. (2019).
[30] S. Bilal, M. Sohail, R. Naz, M.Y. Malik, M. Alghamdi, Upshot of ohmically dissipated Darcy-Forchheimer slip flow of magnetohydrodynamic Sutterby fluid over radiating linearly stretched surface in view of Cash and Carp method, Appl. Math. Mech. 40 (6) (2019) 861–876.
[31] A. Ali, M. Nazir, M. Awais, Aqsa, M.Y. Malik, Stratification phenomenon in an inclined rheology of UCM nanomaterial, Phys. Lett. A 383 (18) (2019) 2201–2206.
[32] M. Ijaz, M. Ayub, Nonlinear convective stratified flow of Maxwell nanofluid with activation energy, Heliyon (2019), e01121.
[33] M. Khan, T. Salahuddin, A. Tanveer, M.Y. Malik, A. Hussain, Change in internal energy of thermal diffusion stagnation point Maxwell nanofluid flow along with solar radiation and thermal conductivity, Chin. J. Chem. Eng. (2018).

[34] A. Alsabery, H. Saleh, I. Hashim, Effects of viscous dissipation and radiation on MHD natural convection in oblique porous cavity with constant heat flux, Adv. Appl. Math. Mech. 9 (2) (2017) 463–484.
[35] K.U. Rehman, M.S. Alqarni, R. Mahmood, N. Kousar, M.Y. Malik, A classical remark on compatibility of an inlet velocity and pressure singularities: finite element visualization, Eur. Phys.J. Plus 134 (2019) 230.
[36] M. Khan, M.Y. Malik, T. Salahuddin, Farzana Khan, Generalized diffusion effects on Maxwell nanofluid stagnation point flow over a stretchable sheet with slip conditions and chemical reaction, J. Braz. Soc. Mech. Sci. Eng. 41 (3) (2019).
[37] M. Ijaz, M. Ayub, M.Y.H. Khan, A. Shaban, Entropy analysis in nonlinearly convective flow of Sisko model in presence of Joule heating and activation energy: buongiorno model, Phys. Scr. (2019).
[38] M. Ijaz, M. Ayub, Activation energy and dual stratification effects for Walter-B fluid flow in view of Cattaneo-Christov double diffusion, Heliyon 5 (2019), e01815.
[39] M. Khan, M.Y. Malik, T. Salahuddin, S. Saleem, A. Hussain, Change in viscosity of Maxwell fluid flow due to thermal and solutal stratifications, J. Mol. Liq. 288 (2019) 110970.
[40] M. Khan, T. Salahuddin, M.Y. Malik, Implementation of Darcy–Forchheimer effect on magnetohydrodynamic Carreau–Yasuda nanofluid flow: application of Von Kármán, Can. J. Phys. 97 (6) (2019) 670–677.
[41] M. Javed, A.A. Alderremy, M. Farooq, Aisha Anjum, S. Ahmad, M.Y. Malik, Analysis of activation energy and melting heat transfer in MHD flow with chemical reaction, Eur. Phys. J. Plus (2019) 134–256.
[42] Mair Khan, Arif Hussain, M.Y. Malik, T. Salahuddin, Shaban Aly, Numerical analysis of Carreau fluid flow for generalized Fourier's and Fick's laws, Appl. Numer. Math. 144 (2019) 100–117.
[43] K.U. Rehman, M.Y. Malik, Waqar A. Khan, Ilyas Khan, S.O. Alharbi, Numerical solution of non-Newtonian fluid flow due to rotatory rigid disk, Symmetry 11 (5) (2019) 699.
[44] T. Salahuddin, Anum Tanveer, M.Y. Malik, Homogeneous-heterogeneous reaction effects in flow of tangent hyperbolic fluid on a stretching cylinder, Can. J. Phys. (2018).
[45] K. U Rehman, Q.M. Al-Mdallal, M.Y. Malik, Symmetry analysis on thermally magnetized fluid flow regime with heat source/sink, Case Stud. Ther. Eng. 14 (2019) 100452.
[46] K.U. Rehman, I. Shahzadi, M.Y. Malik, Q.M. Al-Mdallal, M. Zahri, On heat transfer in the presence of nano-sized particles suspended in a magnetized rotatory flow field, Case Stud. Thermal Eng. 14 (2019) 100457.
[47] M. Khan, T. Salahuddin, M.Y. Malik, F. Khan, Arrhenius activation in MHD radiative Maxwell nanoliquid flow along with transformed internal energy, Eur. Phys. J. Plus 134 (2019) 198.
[48] Z. Abbas, M. Sheikh, Numerical study of homogeneous-heterogeneous reactions on stagnation point flow of ferrofluid with non-linear slip condition, Chin. J. Chem. Eng. 25 (2017) 11–17.
[49] T. Hayat T. Muhammad, A. Alsaedi, On three-dimensional flow of couple stress fluid with Cattaneo-Christov heat flux Chin, J. Phys. 55 (2017) 930–938.
[50] M. Ijaz, M. Ayub, M. Zubair, A. Riaz, On stratified flow of ferromagnetic nanofluid with heat generation/absorption, Phys. Scr. (2018).
[51] M. Ijaz, M. Ayub, H. Khan, Entropy generation and activation energy mechanism in nonlinear radiative flow of Sisko nanofluid: rotating disk, Heliyon (2019), e01863.
[52] R. Malik, M. Khan, Numerical study of homogeneous-heterogeneous reactions in Sisko fluid flow past a stretching cylinder, Results Phys. 8 (2018) 64–70.
[53] A. Hussain, S. Ameer, F. Javed, M.Y. Malik, Rheological analysis on non-Newtonian wire coating, J. Braz. Soc. Mech. Sci. Eng. 41 (2019) 115.
[54] K.U. Rehman, M.Y. Malik, I. Zehra, M.S. Alqarni, Group theoretical analysis for MHD flow fields: a numerical result, J. Braz. Soc. Mech. Sci. Eng. 41 (2019) 156.
[55] S.J. Liao, Homotopy Analysis Method in Non-linear Differential Equations, Springer and Higher Education Press, Heidelberg, 2012.
[56] M. Turkyilmazoglu, Determination of the correct range of physical parameters in the approximate analytical solutions of nonlinear equations using the Adomian decomposition method, Mediterr. J. Math. 13 (6) (2016) 4019–4037.
[57] N. Acharya, K. Das, P.K. Kundua, Cattaneo–Christov intensity of magnetized upper-convected Maxwell nanofluid flow over an inclined stretching sheet: a generalized Fourier and Fick's perspective, Int. J. Mech. Sci. 130 (2017) 167–173.
[58] W.A. Khan, I. Pop, Boundary-layer flow of a nanofluid past a stretching sheet, Int. J. Heat Mass Transf. 53 (2010) 2477–2483.
[59] Kai-Long Hsiao, Stagnation electrical MHD nanofluid Mixed convection with slip boundary on a Stretching Sheet, Appl. Therm. Eng. 98 (2016) 850–861.